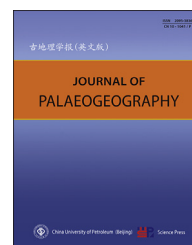




Available online at www.sciencedirect.com

ScienceDirect

journal homepage: <http://www.journals.elsevier.com/journal-of-palaeogeography/>



Geochemistry and sedimentary environments

Testing optically stimulated luminescence dating on sand-sized quartz of deltaic deposits from the Sperchios delta plain, central Greece



Evangelos Tsakalos^{a,b,c,*}, *Elias Dimitriou*^a,
Maria Kazantzaki^b, *Christos Anagnostou*^d,
John Christodoulakis^{b,e}, *Eleni Filippaki*^b

^a Hellenic Centre for Marine Research, Institute of Inland Waters, Anavissos 190 13, Greece

^b Laboratory of Archaeometry, Institute of Nanoscience and Nanotechnology, National Centre for Scientific Research, N.C.S.R. "Demokritos", Agia Paraskevi, Athens 153 10, Greece

^c Department of Geophysics, Division of Earth and Planetary Sciences, Graduate School of Science, Kyoto University, Kyoto 606-8502, Japan

^d Hellenic Centre of Marine Research, Institute of Oceanography, Anavissos 190 13, Greece

^e Climate Research Group, Division of Environmental Physics and Meteorology, Faculty of Physics, National and Kapodistrian University of Athens, Athens 157 84, Greece

Abstract This study reports on the first investigation into the potential of luminescence dating to establish a chronological framework for the depositional sequences of the Sperchios delta plain, central Greece. A series of three borehole cores (20 m deep) and two shallow cores (4 m deep), from across the delta plain, were extracted, and samples were collected for luminescence dating. The luminescence ages of sand-sized quartz grains were obtained from small aliquots of quartz, using the Single-Aliquot Regenerative-dose (SAR) protocol. The equivalent dose determination included a series of tests and the selection of the Minimum Age Model (MAM) as the most appropriate statistical model. This made it possible to confirm the applicability of quartz Optically Stimulated Luminescence (OSL) dating to establish absolute chronology for deltaic sediments from the Sperchios delta plain.

Testing age results of the five cores showed that the deltaic sediments were deposited during the Holocene. A relatively rapid deposition is implied for the top ~14 m possibly as a result of the deceleration in the rate of the sea-level rise and the transition to terrestrial conditions, while on the deeper parts, the reduced sedimentation rate may indicate a lagoonal or coastal environment.

* Corresponding author.

E-mail address: e.tsakalos@inn.demokritos.gr (E. Tsakalos).

Peer review under responsibility of China University of Petroleum (Beijing).

<https://doi.org/10.1016/j.jop.2018.01.001>

2095-3836/© 2018 China University of Petroleum (Beijing). Production and hosting by Elsevier B.V. on behalf of China University of Petroleum (Beijing). This is an open access article under the CC BY-NC-ND license (<http://creativecommons.org/licenses/by-nc-nd/4.0/>).

Keywords Luminescence dating, Holocene, Sedimentation rates, Deltaic deposits, Sperchios delta plain, Central Greece

© 2018 China University of Petroleum (Beijing). Production and hosting by Elsevier B.V. on behalf of China University of Petroleum (Beijing). This is an open access article under the CC BY-NC-ND license (<http://creativecommons.org/licenses/by-nc-nd/4.0/>).

Received 8 May 2017; accepted 8 January 2018; available online 11 January 2018

1. Introduction

During the last few decades, many studies have been conducted regarding the Holocene stratigraphic configuration of several deltaic successions around the Mediterranean (e.g., Amorosi *et al.*, 2005; Boyer *et al.*, 2005; Bruno *et al.*, 2015; Pechlivanidou *et al.*, 2014). The majority of the research is confined to seismic profile interpretations (e.g., Lafuerza *et al.*, 2005; Somoza *et al.*, 1998; Styllas, 2014), geochemical and sedimentological studies (e.g., Pechlivanidou *et al.*, 2014), and tectonics and geodynamics (e.g., Lafuerza *et al.*, 2005; Somoza *et al.*, 1998; Styllas, 2014).

The Sperchios delta plain is located in central Greece and covers an area of 121.5 km². Several times in the past, the river's main channel shifted its course due to hydrological changes or tectonic activity in the Sperchios basin. These changes on the river's channel resulted in the development of many deltaic prolongations in the Maliakos Gulf and created an extensive deltaic plain due to the high rates of sedimentation (Poulos *et al.*, 1997).

Previous studies in the Sperchios delta plain have mainly been conducted regarding the palaeogeography of the battle terrain in ancient Thermopylae, particularly concerning the reconstruction of the shoreline position at the time of the battle (Kraft *et al.*, 1987; Tziavos, 1977; Vouvalidis *et al.*, 2010a). More recently, the palaeogeography of the Late Holocene Sperchios delta plain has been outlined by Pechlivanidou *et al.* (2014), with sedimentological, palaeontological, geochemical, and mineral magnetic property approaches to detect the palaeoenvironmental signal of Sperchios deltaic deposits. In this study it was estimated that the transition from lagoonal to terrestrial conditions and the development of the Sperchios delta plain took place around ~6000 cal yr BP (Pechlivanidou *et al.*, 2014) following the slowing rate of sea-level change as recorded across the broader region of the Aegean (Lambeck and Purcell, 2005; Pavlopoulos, 2010; Pavlopoulos *et al.*, 2012).

However, little effort has been made so far to reconstruct the comprehensive and sequential history

of the upper part of the Sperchios delta plain based on numerical age data, with the available ages mainly based on archaeological and radiocarbon dates which bear a range of limitations and uncertainties (e.g., sample contamination and inaccurate estimation of the ratio of ¹⁴C–¹²C). Previous chronological studies for the delta (Pechlivanidou *et al.*, 2014; Vouvalidis *et al.*, 2010b) remain limited in literature. Thus, a systematic application of dating techniques is required, which would provide an insight into the Holocene geomorphologic history of the area by establishing the chronology of the region.

Over the last three decades luminescence dating methods have been developed and now they are widely applied to dating sediments from different geological environments (e.g., aeolian, fluvial and marine). In recent years, OSL (Optically Stimulated Luminescence) dating of fluvial deposits has gained much attention (e.g., Theodorakopoulou *et al.*, 2009; Zacharias *et al.*, 2009) because of the advantage of directly determining the time elapsed since deposition, thus avoiding indirect dating using radiocarbon or other methods (e.g., Wallinga and Bos, 2010; Wallinga *et al.*, 2010). Detailed reviews on the application of OSL dating on fluvial sediments are given in Wallinga (2002) and Rittenour (2008).

Although OSL dating is now widely applied to a wide range of sedimentary environments, its application on fluvial deposits is still limited, since such deposits may have the problem of incomplete bleaching of grains. Grains transported by fluvial processes may not be fully bleached, as water turbulence and short transportation do not allow for a complete resetting of the OSL signal (Ditlefsen, 1992; Rendell *et al.*, 1994). During burial diagenesis, the OSL signal builds up again adding to a residue signal and resulting in a broad distribution of the equivalent dose (D_E).

A number of different methodologies that can assist in obtaining the best estimate of D_E are nowadays available (e.g., Lepper and McKeever, 2002; Olley *et al.*, 1998; Stokes *et al.*, 2001), and of these the most widely used, are the “age models” of Galbraith *et al.* (1999). These models are based on statistical analysis of the D_E values and their validity has been

demonstrated in empirical and modeling studies (e.g., Arnold *et al.*, 2009; Bailey and Arnold, 2006). Galbraith and Roberts (2012) provide a review of the statistical characteristics that are used to obtain the best D_E value.

In this study, we investigate the applicability of OSL dating on sand-sized quartz to construct a reliable chronological framework for the upper (~20 m) sediments of the Sperchios delta plain. Here we present a new chronology for the Sperchios delta plain and provide sedimentation rates of its depositional sequences during the Holocene. Taking into account that limited light exposure prior to deposition and burial of the quartz grains may result in incomplete resetting of the OSL signal, we employed statistical approaches for obtaining reliable D_E estimates.

2. Study area and core description

The Sperchios delta plain embraces part of an active rift system formed by an extensional deformation of the Greek mainland since the Early Pliocene (~5 Ma) (Kilias *et al.*, 2008). The rift was characterized by an asymmetric half-graben (Eliet and Gawthorpe, 1995) mainly controlled by movements of its active fault boundary along its southern margin. The main fault system which has determined the topography of the area is located in the southern part of the Sperchios basin and can be subdivided into two different parts: (1) the Sperchios–Ipati fault zone located in the west, abutting the valley of the Sperchios River to the south, and (2) the Kamena Vourla–Arkitsa fault zone in the east, abutting the Maliakos basin to the south (Eliet and Gawthorpe, 1995; Kilias *et al.*, 2008). Fault tectonism took place at the end of the Pliocene and the beginning of the Pleistocene periods, and continues to the present. Due to neotectonic movements, the Pliocene deposits developed in the south of the Maliakos Gulf, had been uplifted by more than 500 m (Gartzos and Stamatis, 1996; Maroukian and Lagios, 1987), where a vertical displacement of about 1800 m has been suggested for the southern boundary of the Sperchios River catchment area, as a result of intense tectonic activity during the Quaternary (Maroukian and Lagios, 1987).

The Sperchios basin chiefly comprises the Paleocene–Eocene flysch formations, mainly appearing in the western and southern parts of the basin (~46% of the total area). Extended limestone formations can be found in the eastern and southern parts of the basin (~14% of the total area), while ophiolite and molasse formations cover the central mountainous

part (~11% of the total area). The Sperchios River valley area, as the central part, is covered by the Quaternary unconsolidated fluvial deposits, including the Holocene deltaic sequences (Fig. 1).

Previous studies have indicated that terrestrial sediments were found at the deepest parts (~40 m.b.s.l.) in the central part of the present Sperchios delta plain and represent fluvial sediments accumulated probably during the Late Quaternary or during the earliest stage of the last transgression around the Pleistocene–Holocene boundary, when the rate of sea-level rise was outpaced by the sediment accumulation rate (Pechlivanidou *et al.*, 2014).

Sea-level rise during the Early Holocene (Lambeck and Purcell, 2005; Pirazzoli, 1996; Vouvalidis *et al.*, 2005) flooded the area of the present delta plain and created sediment successions comprising coastal sediments and distal prodelta deposits (Pechlivanidou *et al.*, 2014). During the Middle–Late Holocene, deceleration in sea-level rise favored the progradation of the Sperchios delta and a shift back to terrestrial conditions, as sediment supply exceeded the relative rate of sea-level rise.

Different sedimentary facies represent different palaeoenvironmental changes across the Sperchios delta plain. Terrestrial sediments represent the fluvial processes, while, the presence of molluscan shell fragments probably indicates the rising sea-level conditions and a coastal environment. Our research samples, extracted through coring described as below, comprise the sedimentary facies of the Holocene transgressive–regressive strata overlying the Late Pleistocene deposits that followed the general stratigraphic development of the Holocene Mediterranean deltas (Stanley and Warne, 1994). Selections of coring locations were based on the proximity of each borehole to the Sperchios River and current coastline, to achieve a good representation of the diachronic sedimentary processes that have taken place in the Sperchios basin. And, the Holocene depositional sequences of the Sperchios delta plain were studied on the basis of samples from these five cores (Fig. 1).

The basic information of the five cores is given in Table 1.

Coring instruments included a truck-mounted hydraulic rotary rig with an auger being pushed in using hydraulic power or percussion, if needed (Fig. 2a) and a vibra coring unit with a vibrating motor used to assist in driving the core barrel into the sediment (Fig. 2b). The auger used a 7.5 cm lined bore. Throughout the drilling operation, the boreholes were sleeved in order to prevent the collapse of sediment into the borehole and avoid sampling disturbed sediments. The retrieved core samples were immediately capped.

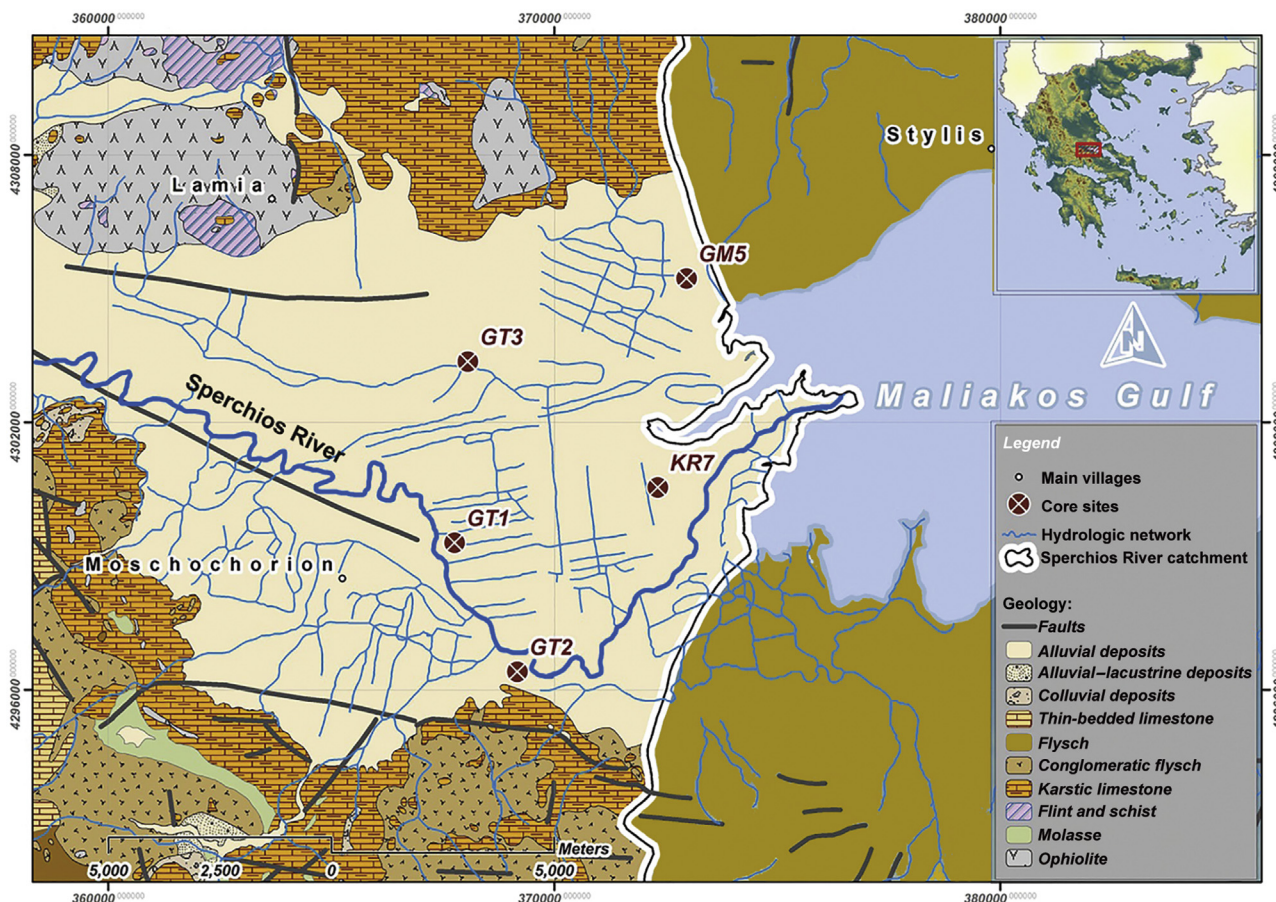


Fig. 1 Geologic map of the study area and geographic sampling sites of the five cores, Sperchios delta plain, central Greece (with the Gauss plane rectangular coordinate system; modified from Marinou *et al.*, 1963, 1967).

Three cores were derived from the central part of the Sperchios delta plain using the truck-mounted hydraulic rotary rig and two cores were from the lower part of the Sperchios delta plain by vibra coring; the maximum drilling length was 20 m. All core depths are recorded as meters below sea-level (m.b.s.l.). A simplified diagrammatic representation of these five cores is provided in Fig. 3, based on macroscopic observations and grain-size analyses.

During macroscopic observations, attention was usually paid to sediment color, grain size, textures, structures, etc. Regarding grain-size analyses, since that no continuous sampling was executed over the full cores length, it is impossible to discuss detailed grain-size grading trends. Sample selections for grain-size analyses as well as for luminescence dating were based on macroscopic observations (distinct sedimentary layers). In total, 31 samples were collected for grain-size analyses. Grain-size analyses were conducted at the laboratory of sedimentology of the Hellenic Centre for Marine Research (“H.C.M.R.”), and using the Micromeritics® SediGraph 5100 device. The lithological characterization of each sample was obtained using triangular charts (Folk, 1974). The results of grain-size analyses along with their lithological characterization are shown in Table 2 and Fig. 3. Sediment color was distinguished visually by comparison with standard Munsell Soil Color Charts (Munsell color company, 1994) and is reported in general terms.

In total, 19 samples were collected from the five cores at varying depths, among which the deepest one

Table 1 The basic information of the five cores extracted from the Sperchios delta plain.

Core ID	Latitude–longitude coordinates	Elevation (m.b.s.l.)	Maximum core length (m)
GT1	38°49'57"N 22°28'35"E	6	20
GT2	38°48'24"N 22°29'36"E	11	17.7
GT3	38°52'08"N 22°28'45"E	2	13.8
GM5	38°53'12"N 22°32'06"E	0.3	3.9
KR7	38°50'39"N 22°31'43"E	1	3.1

Note: m.b.s.l. = meters below sea-level.



Fig. 2 Drilling operation scene and coring instruments: (a) the truck-mounted hydraulic rotary rig and (b) the vibra coring.

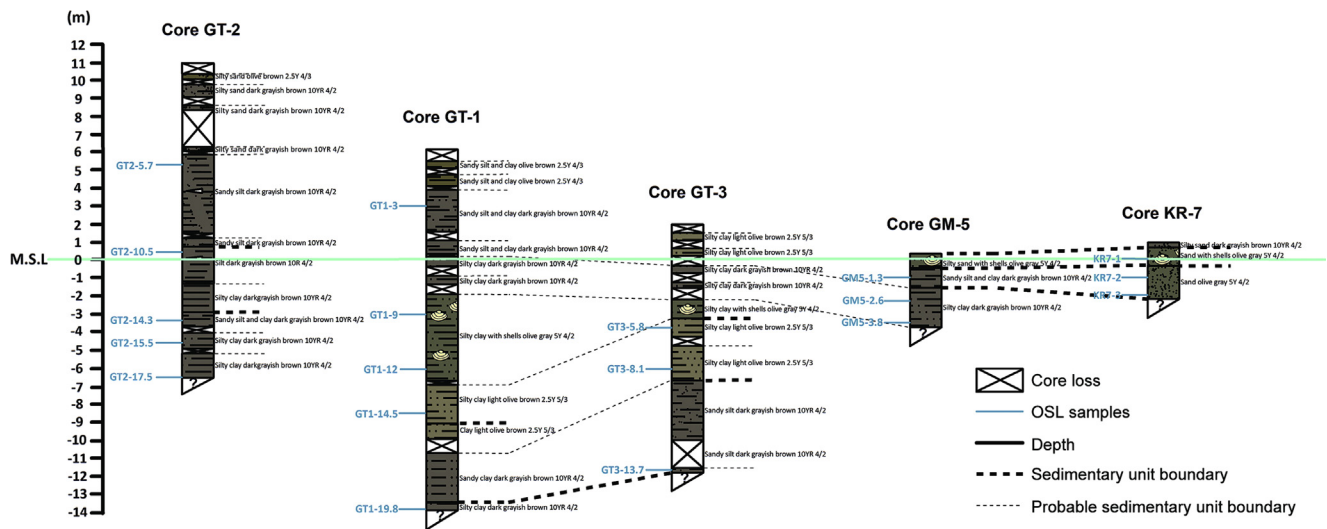


Fig. 3 Sedimentary facies of the five cores from the Sperchios delta plain based on macroscopic observations and grain-size analyses. The sampling spots (e.g., GT1-3) for luminescence dating are indicated by laboratory codes.

Table 2 Grain-size analyses of the five cores along with their lithological characterizations.

Sample	Sand (%)	Silt (%)	Clay (%)	Lithological characterization
GT1-1.7	12.8	38.0	49.2	Sandy silty clay
GT1-3	15.2	35.4	49.4	Sandy silty clay
GT1-6.5	6.2	39.1	54.7	Silty clay
GT1-9	7.8	37.2	55.0	Silty clay
GT1-12	1.1	49.8	49.1	Silty clay
GT1-13.5	4.3	45.5	50.2	Silty clay
GT1-14.5	6.5	38.1	55.4	Silty clay
GT1-15.2	1.5	23.5	75.0	Clay
GT1-17.3	38.2	18.7	43.1	Sandy clay
GT1-19.8	2.3	54.2	43.5	Silty clay
GT2-0.8	74.3	20.6	5.1	Silty sand
GT2-5.7	9.8	60.5	29.7	Sandy silt
GT2-10.5	3.8	68.1	28.1	Silt
GT2-13.4	8.1	38.2	53.7	Silty clay
GT2-14.3	44.8	33.1	22.1	Sandy silty clay
GT2-15.5	9.8	56.3	33.9	Silty clay
GT2-17.5	2.7	58.4	38.9	Silty clay
GT3-1.3	7.7	39.1	53.2	Silty clay
GT3-2.3	8.1	35.4	56.5	Silty clay
GT3-4.8	8.8	58.7	32.5	Sandy silt
GT3-5.8	4.5	56.1	39.4	Silty clay
GT3-8.1	4.7	58.3	37.0	Silty clay
GT3-13.7	16.6	60.3	23.1	Sandy silt
GM5-0.5	62.8	10.2	27.0	Silty sand
GM5-1.3	13.3	37.5	49.2	Sandy silty clay
GM5-2.6	6.4	37.7	44.1	Silty clay
GM5-3.8	4.8	57.1	38.1	Silty clay
KR7-0.2	70.1	22.3	7.6	Silty sand
KR7-1	79.5	17.2	3.3	Sand
KR7-2	83.7	10.8	5.5	Sand
KR7-3	89.2	7.3	3.5	Sand

was up to 14 m.b.s.l. (Fig. 3, GT1-19.8), for optically stimulated luminescence dating.

3. Luminescence dating

3.1. Sample preparation and measurement facilities

Samples collected from the five cores were submitted to the Luminescence Dating Laboratory of the National Centre for Scientific Research, “Democritos” Greece, where they were opened under subdued red light conditions to obtain samples for OSL analysis. For each core sample, one half was brought into light for macroscopic observations and grain-size analyses, and at the same time, to select suitable depth intervals for OSL sampling. However, the OSL samples were taken from the other half of the core.

We tried to sample sandy intervals and avoid sampling closely to the interval boundaries to facilitate

reliable estimation of the gamma dose rate. Each sample taken for luminescence dating represents ~8 cm of core length. The outer 1 cm of the sediments was discarded to avoid possible contamination of disturbed sediments while recovering the core.

Quartz is commonly the preferable mineral in OSL dating of fluvial deposits, as its residual signals are usually lower than those for feldspar (e.g., Fiebig and Preusser, 2007), and the quartz OSL signal is more stable over geological timescales (Wintle and Murray, 2006). We chose sand-sized grains for D_E determination as these allow OSL measurements on aliquots containing only a few grains, which facilitates better interpretation of the completeness of OSL resetting prior to deposition and burial (e.g., Duller, 2008).

Following conventional laboratory practices (e.g., Preusser *et al.*, 2008), quartz coarse-grains were prepared using the procedure of chemical treatment with 10% hydrochloric acid to remove carbonate cements and 10% hydrogen peroxide to remove organic content, and then were dried and sieved. Fractions were treated with 40% hydrofluoric acid to avoid contribution of the alpha-irradiated outer part of the mineral, followed by a rinse with 10% hydrochloric acid to remove fluorosilicate and a final sieving to separate traces of any remnant byproducts. Purified quartz grains which were treated with 40% hydrofluoric acid for 90 min to remove all other minerals mainly fell in the range of 80–125 μm .

Single aliquot measurements carried out on small aliquots are assumed better to reflect any inhomogeneities in the equivalent dose distribution than using larger aliquots (e.g., Fuchs and Wagner, 2003; Olley *et al.*, 1998). Thus, for each sample, at least 12 aliquots were measured using aliquots with only the central 2 mm diameter covered with quartz grains.

Measurements were carried out on a Risø TL-DA 15 luminescence reader fitted with a Thorn EMI photomultiplier tube. Irradiation was from a calibrated $^{90}\text{Sr}/^{90}\text{Y}$ β source. Blue LEDs (470 nm) were used for stimulating the aliquots and a 7.5 mm Hoya U-340 filter was the signal detection filter mounted in front of the photomultiplier tube. The single-aliquot regenerative-dose (SAR) protocol after Murray and Wintle (2003) was applied for D_E measurements (Table 3).

3.2. Dose rate determination

To avoid potential problems related to an inhomogeneous gamma radiation field, OSL samples were taken from thick lithological-homogeneous sediment layers and far from lithological boundaries. Besides, a separate sample for dose rate analysis was taken over the entire range of the luminescence sample.

Table 3 The single-aliquot regenerative-dose (SAR) protocol applied for this study to quartz grains.

Step	Treatment
1	Give dose
2	Preheat, 10 s at 240 °C
3	Blue-LED stimulation, 40 s at 125 °C
4	Give test dose
5	Cut-heat, 0 s at 200 °C
6	Blue-LED stimulation, 40 s at 125 °C
7	IR diodes stimulation, 100 s at 125 °C
8	Return to Step 1

The calculation of the dose rates (U, Th, K) was based on analytical data obtained by Inductively Coupled Plasma Mass Spectrometry (ICP-MS; ACME laboratories, Canada) and using the “The Dose Rate calculator” (DRc) software developed by Tsakalos *et al.* (2016). The DRc uses the conversion factors proposed by Guérin *et al.* (2011) and the attenuation factors (due to water content) for alpha radiation by Aitken (1985), beta radiation by Nathan and Mauz (2008), and gamma radiation by Guérin and Mercier (2012). DRc also calculates the cosmic ray contribution to the total dose rate according to Prescott and Stephan (1982) and Prescott and Hutton (1988, 1994) using the altitude and latitude of the sampling site, its present-day depth and the density of the overburden. The final dose rates are obtained by correcting for the acid etching of grains and the grain size. Sediment water content was determined using the

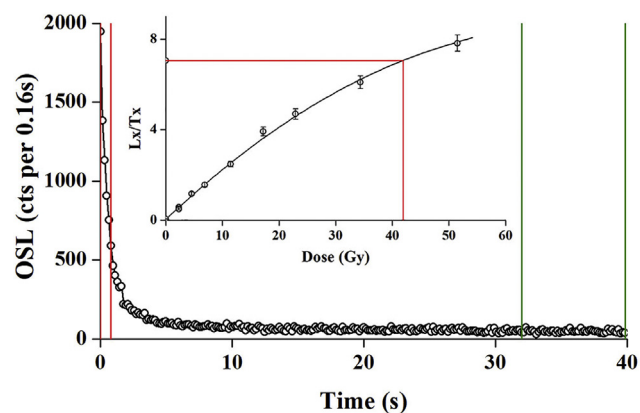


Fig. 4 Representative luminescence decay curve and corresponding sensitivity-corrected dose response curve for one aliquot from quartz of sample GT1-19.8. The vertical red lines indicate the initial integral signal (0.8 s) which was used to obtain the luminescence signal, while the green lines indicate the time interval (last 8 s) used for background subtraction.

present water content with an error of $\pm 5\%$ and considered to remain constant during burial. The dose rates are listed in Table 4.

3.3. OSL measurements

A typical decay and a dose–response curve for one aliquot (sample GT1-19.8) from the coarse-grain (80–125 μm) quartz is shown in Fig. 4. A measure of the residual IRSL (infrared stimulated luminescence)

Table 4 The dose rate (U, Th, K) calculation to quartz grains with 80–125 μm size from OSL samples.

Sample	U (ppm)	Th (ppm)	K (wt%)	Cosmic ray radiation (Gy)	Depth (m)	Water content (wt%)	Total dose rate (Gy/ka)
GT1-3	1.9	8.6	2.2	0.09	3	27.8	2.56 ± 0.03
GT1-9	1.9	9.6	2.5	0.04	9	33	2.67 ± 0.04
GT1-12	1.6	8.1	2.4	0.03	12	34.7	2.42 ± 0.04
GT1-14.5	1.9	8.9	2.4	0.02	14.5	36.3	2.48 ± 0.03
GT1-19.8	2.1	9.5	2.7	0.01	19.8	39.3	2.66 ± 0.03
GT2-5.7	1.1	4.1	1.3	0.06	5.7	34.1	1.39 ± 0.02
GT2-10.5	1.2	4.2	0.9	0.03	10.5	35.8	1.09 ± 0.01
GT2-14.3	1.5	5.6	1.5	0.02	14.3	39.2	1.58 ± 0.02
GT2-15.5	1.7	7.4	2.4	0.02	15.5	39.6	2.29 ± 0.03
GT2-17.5	2.2	8.2	2.6	0.02	17.5	39.9	2.51 ± 0.04
GT3-5.8	2.6	9.1	2.9	0.06	5.8	33.6	2.91 ± 0.25
GT3-8.1	2.4	9.1	2.7	0.04	8.1	35.1	2.83 ± 0.04
GT3-13.7	1.8	7.6	1.7	0.02	13.7	39.9	1.88 ± 0.03
GM5-1.3	2.0	7.8	2.2	0.12	1.3	38.3	2.36 ± 0.03
GM5-2.6	1.7	7.1	1.9	0.10	2.6	39.7	2.01 ± 0.03
GM5-3.8	1.7	5.9	1.5	0.09	3.8	40.3	1.70 ± 0.03
KR7-1	1.4	4.0	1.4	0.12	1	38.4	1.51 ± 0.02
KR7-2	1.6	4.9	1.4	0.10	2	37.6	1.58 ± 0.02
KR7-3	1.3	4.9	1.3	0.09	3	40	1.43 ± 0.02

Note: The depths were measured as from the surface.

to detect feldspar contamination was also incorporated at the end of each sequence. No signal response was observed during infrared stimulation, which was carried out for each aliquot at the end of a measurement sequence. Therefore, it is concluded that a significant feldspar contamination is unlikely in the quartz samples investigated in this study.

3.3.1. Validation tests

Prior to standard dating using the SAR procedure, the performance of the protocol parameters was confirmed by a preheat plateau test (Murray and Wintle, 2000) and a dose recovery test (Murray and Wintle, 2003) (Figs. 5–7).

As shown in the steps of the SAR protocol (Table 3), a high temperature is applied before the Blue-LED stimulation. This is necessary so that electrons accumulated in any thermally unstable traps will be thermally stimulated and released, preventing their unwanted contribution to the stable OSL signal that will be measured in the next step of the SAR protocol. If an unwanted signal contributes to the OSL signal, it will result in an increased D_E and therefore get a wrong overestimated age. A preheat plateau test shows that

if there is any unwanted contribution to the stable OSL signal, it will cause erroneous D_E determination (Wintle and Murray, 2006). In the preheat test, a number of D_E values are determined using different preheat temperatures (Murray and Wintle, 2000; Roberts *et al.*, 1999); and the preheat temperature which is taken for measurement should be obtained in a plateau. Since the examined samples may be bleached, the scattered D_E distribution would be expected, thus obtaining the right preheat plateau is difficult. In this study we used a combination of preheat and dose recovery test which can overcome this problem. For this test, aliquots of two samples were bleached in the OSL reader using Blue-LEDs for 40 s to reset the natural signal (e.g., Athanassas, 2011; Kunz *et al.*, 2013; Trauerstein *et al.*, 2017). The bleached aliquots were then irradiated with a fixed β -dose of 11.5 Gy and measured at various preheat temperatures (20 °C spacing) ranging from 200 °C to 300 °C with a cut-heat at 200 °C. The measured (or recovered) dose is almost equal to the given dose, *i.e.*, the ratio of the measured dose *versus* the given dose is close to unity (value of 1), between temperatures 220 °C and 240 °C (Fig. 5), and the former temperature was selected for the subsequent measurements. The

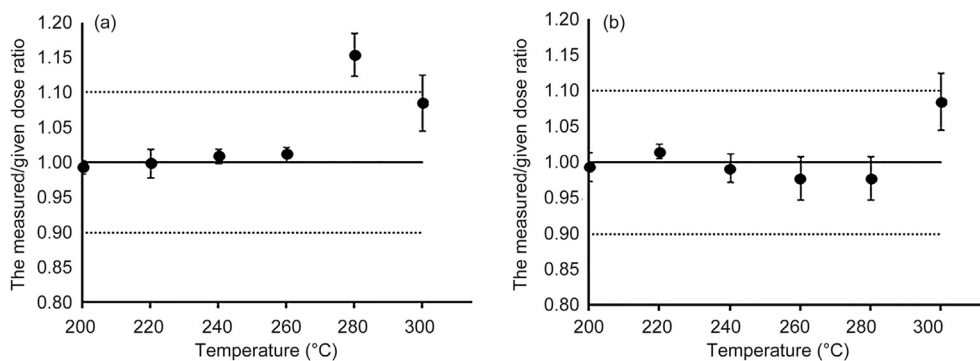


Fig. 5 Results of the preheat-dose recovery test performed for quartz from samples (a) GT1-3 and (b) GT2-17.5. Aliquots were measured in groups of three using six different preheat temperatures from 200 °C up to 300 °C (held for 10 s each). Black dots indicate the measured/given dose ratios calculated for each group. The target value is unity (black line). The range of acceptability is between 0.9 and 1.1 (dotted lines). The results were checked for sensitivity changes.

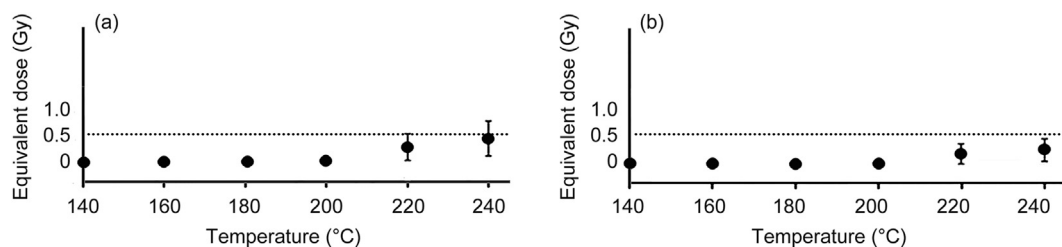


Fig. 6 Results of the cut-heat test performed for quartz from samples (a) GT1-3 and (b) GT2-17.5. The results were checked for sensitivity changes.

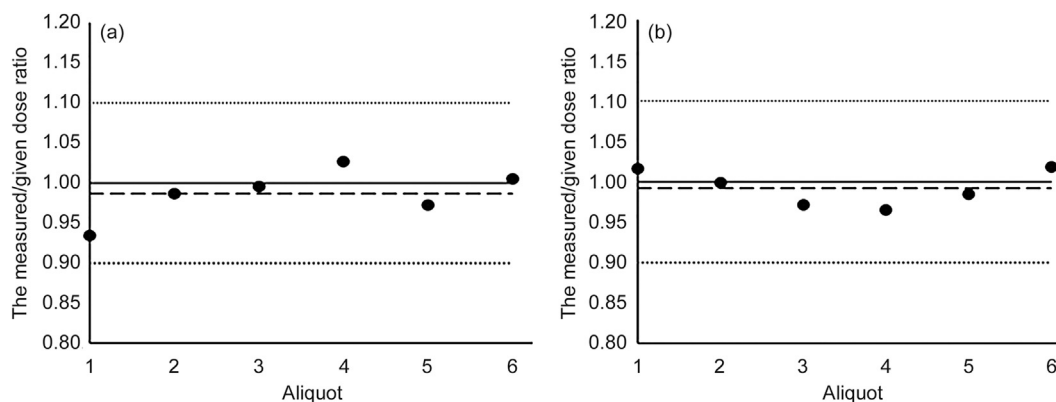


Fig. 7 Results of the dose recovery test for samples (a) GT1-3 and (b) GT2-17.5. Six aliquots for each sample were measured. Black dots indicate the measured/given dose ratios calculated for each aliquot. The target value is unity (black line). The range of acceptability is between 0.9 and 1.1 (dotted lines). The dashed line shows the mean ratio ($N = 6$) of the given dose to the recovered D_E . The results were checked for sensitivity changes.

recycling ratios were systematically consistent with unity (ranging from 0.98 to 1.05) and the recuperation never exceeded 2%.

Many chronological studies (*e.g.*, Madsen *et al.*, 2005; Wintle and Murray, 2006) have shown that quartz samples can be affected by thermal transfer. An approach similar to the preheat-dose recovery test was applied, during which no artificial irradiation was given, at various cut-heat temperatures between 140 °C and 240 °C (with a preheat at 240 °C) to examine if thermal transfer is apparent. Results clearly show that the equivalent dose (D_E) is insensitive to cut-heat temperatures between 140 °C and 200 °C, resulting in the selection of the 200 °C temperature for cut-heat for all quartz samples. And, for cut-heat temperatures from 220 °C to 240 °C, the D_E increased around 0.5 Gy (Fig. 6).

The reliability of these measuring parameters was further confirmed by a dose recovery test undertaken on aliquots from two samples. Six aliquots of sample GT1-3 and six aliquots of GT2-17.5 were bleached by sun exposure for 6 h and then an 11.5 Gy dose was given. SAR protocol was then applied to the test if the 11.5 Gy dose could be recovered. For a well performing SAR protocol, the ratio between the measured dose and the given dose should be close to unity (Murray and Wintle, 2003), at least be in the range of 0.9–1.1. The test showed that recovery ratios were within the 2σ -level (0.9–1.1; Fig. 7). The mean ratio ($N = 6$) of the given dose to the recovered D_E was 0.97 ± 0.03 for sample GT1-3 and 0.98 ± 0.01 for sample GT2-17.5 (Fig. 7; the dashed line), signifying that the SAR protocol generates a well equivalent dose accuracy and precision. Furthermore, all “recycling ratio” values for the same aliquot were within $\pm 5\%$ of unity (mean ratio

0.97 ± 0.04). That is, we consequently performed the SAR protocol as described in Table 3.

4. Results and discussion

4.1. Determination of the D_E value based on statistical models

The establishment of the SAR protocol has revealed that different aliquots of the same sample give different equivalent doses. And this brought up the matter of how the equivalent dose (D_E) distribution of a sample is to be depicted in order to get a meaningful and reliable representation and thus extract the necessary information for age calculations. A simple way of getting a first impression of how the equivalent doses are distributed is to produce a probability density function (PDF). However, the influence that an individual D_E value distributed upon the overall distribution cannot be seen and examined in a single PDF. To avoid the uncertainty inherent in PDFs, Galbraith *et al.* (1999) developed the “radial plot” for the presentation of single-aliquot data.

The variety in D_E distributions can indicate that a sample was subjected to diverse bleaching conditions (Arnold *et al.*, 2007; Olley *et al.*, 1999; Rodnight *et al.*, 2006) and post-depositional processes, and/or millimeter-scale differences in the beta dose rate to individual grains (Jacobs and Roberts, 2007) or even intrinsic differences in the luminescence sensitivity of the measured aliquots.

Dating of deltaic sediments utilizing luminescence techniques could be problematic. Because of the transport–deposition mode of such sediments,

sunlight exposure for the mineral grains might be not long enough to release any stored energy completely from the crystal lattice prior to deposition. In heterogeneously bleached samples, such as fluvial sediments, the D_E distribution generally shows larger variability (e.g., Arnold *et al.*, 2007; Olley *et al.*, 1999; Rodnight *et al.*, 2006). This has brought up the matter of how the best estimate of D_E could be extracted and used for age calculations.

Different approaches and methodologies have been proposed for assisting in obtaining the best estimate of the D_E (e.g., Galbraith *et al.*, 1999; Lepper and McKeever, 2002; Olley *et al.*, 1998; Stokes *et al.*, 2001), and of these the most broadly used are the “Age Models” developed by Galbraith *et al.* (1999). Many studies used over-dispersion values as the only diagnostic criterion for the choice of the most appropriate methodology (e.g., Olley *et al.*, 2004a). This value gives an estimate of the relative standard deviation of the true D_E , remaining after the measurement error of each aliquot has been taken into account; if the measurement error was the only reason for the variation observed in D_E , then the over-dispersion would be zero. Theoretically, for a well-bleached and homogeneous sample, an over-dispersion value close to zero would be expected. However, in a study testing the accuracy of various statistical models, Bailey and Arnold (2006) concluded that the selection of the most appropriate methodology based only on a single descriptor for the D_E distribution (such as the degree of

over-dispersion) is not possible, and that no single analysis method is applicable to all samples from different depositional environments; and they proposed that the decision process should include a series of criteria which could describe the shape of the D_E distribution (skewness, kurtosis, over-dispersion) and the presence of negative D_E values. Bailey and Arnold (2006) also developed a decision process guide (Bailey and Arnold, 2006; page 2500) that can be used to help choose the most suitable methodology on a case-by-case basis.

Based on such considerations, we applied the Minimum Age Model (MAM) suggested by Galbraith *et al.* (1999) to determine the appropriate D_E value. The MAM can be used for heterogeneous bleached samples and can identify the well-bleached aliquots by applying a truncated normal distribution to the log D_E values (Galbraith and Laslett, 1993; Galbraith *et al.*, 1999). The width of this minimum D_E distribution is derived from statistical measurement errors of each D_E value and the over-dispersion.

In our study, the D_E distributions of the measured aliquots clearly show a significant scatter with values of skewness ranging from 0.2 to 2.8, kurtosis ranging from 0.2 to 1.9, and over-dispersion values ranging from 15% to 29% (Table 5), which may be considered as typical for fluvial sediments (e.g., Arnold *et al.*, 2009; Olley *et al.*, 2004b; Rodnight *et al.*, 2006).

Aliquots of two samples are depicted in radial plots along with their MAM calculated D_E value in Fig. 8.

Table 5 Determination of the most appropriate equivalent dose (D_E) using numerical parameters.

Sample	D_E distribution characteristics			D_E value (Gy)		
	Over-dispersion	Skewness	Kurtosis	Mean	Weighted mean ^(a)	MAM value
GT1-3	22%	2.8	-0.5	7.15 ± 2.2	6.1 ± 1.1	5.74 ± 0.83
GT1-9	24%	0.6	-1.6	18 ± 2	13.8 ± 3	12.5 ± 1.43
GT1-12	20%	2.5	-0.7	19 ± 5.7	14.9 ± 1.3	14 ± 1.65
GT1-14.5	19%	1.1	-0.6	21.9 ± 3.3	17.8 ± 2.2	16.9 ± 1.8
GT1-19.8	16%	1.5	-0.2	30.4 ± 8.7	25.5 ± 2.7	23 ± 2.3
GT2-5.7	21%	1.9	1.3	8.2 ± 2.6	6.9 ± 1.1	5.4 ± 0.76
GT2-10.5	17%	1.7	1.3	11.2 ± 1	7 ± 0.3	6.4 ± 0.22
GT2-14.3	24%	1.9	1.6	19.3 ± 1.4	14.3 ± 0.6	11.2 ± 0.4
GT2-15.5	16%	1.9	1.8	25.8 ± 3.2	21.9 ± 1.3	20 ± 1.1
GT2-17.5	18%	1.0	-0.3	47 ± 5.3	40.7 ± 2.9	35.3 ± 2.2
GT3-5.8	24%	0.4	-1.4	18.6 ± 4.1	14.8 ± 2	11.1 ± 1.7
GT3-8.1	28%	1.3	1.9	26.5 ± 4.6	17.1 ± 2.8	12.6 ± 1.6
GT3-13.7	15%	0.4	-0.8	18.1 ± 2.5	15.5 ± 1.8	12.9 ± 1.8
GM5-1.3	27%	0.2	-1.6	4.2 ± 0.7	3.1 ± 0.4	1.7 ± 0.4
GM5-2.6	23%	0.5	1.1	6.3 ± 1.1	4.7 ± 0.8	3.8 ± 0.8
GM5-3.8	26%	1.0	0.3	7.3 ± 1.2	5.8 ± 0.9	5.3 ± 0.9
KR7-1	29%	1.5	0.4	4.6 ± 1.1	2.4 ± 0.4	0.98 ± 0.2
KR7-2	24%	1.5	1.9	5.1 ± 1	3 ± 0.6	1.8 ± 0.5
KR7-3	19%	0.6	-1.1	7.6 ± 1.9	5.1 ± 0.9	3.8 ± 0.7

Note: ^(a) For the weighted mean, each value was weighted by $1/\sigma_{D_E}$.

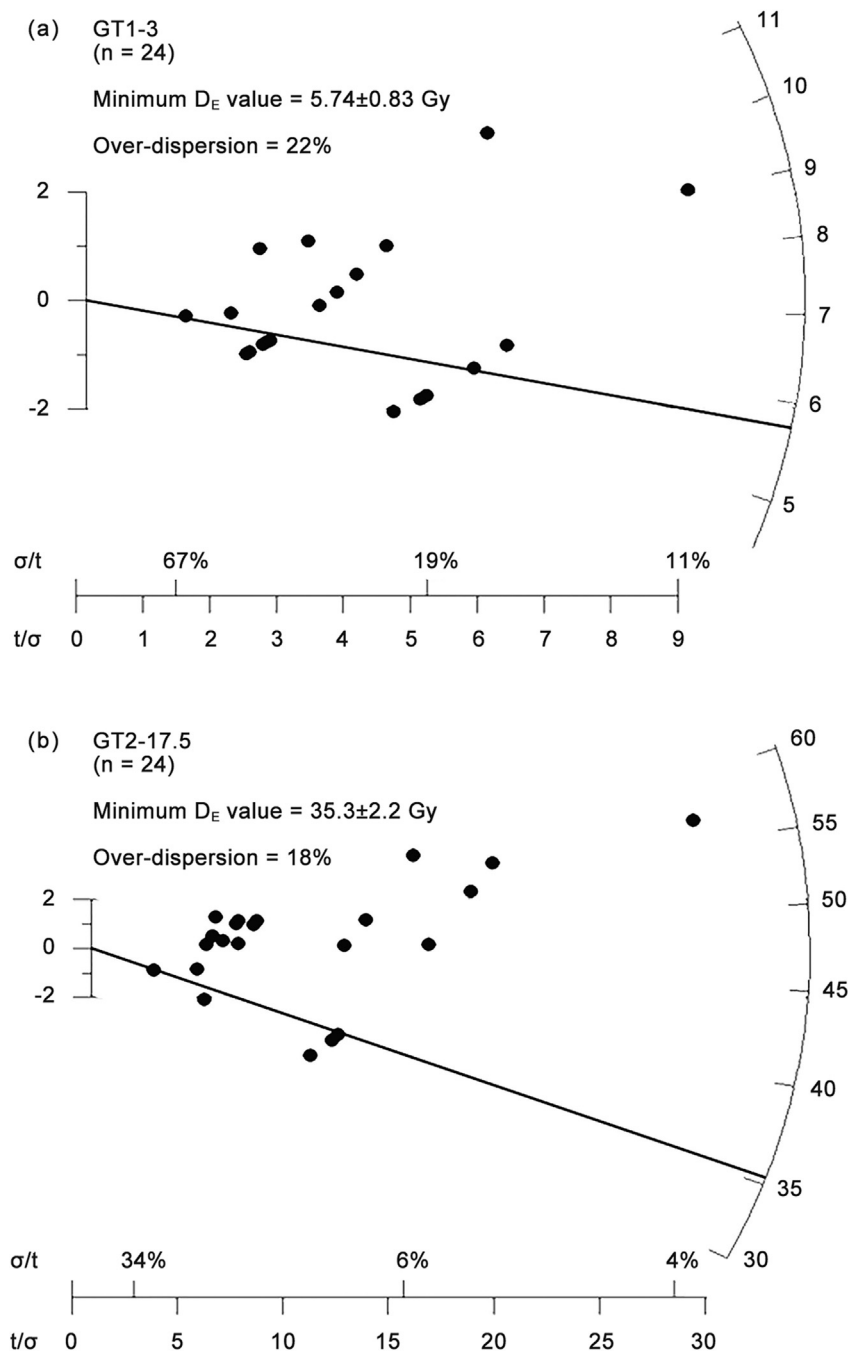


Fig. 8 Radial plots of the D_E values for two samples (a) GT1-3 and (b) GT2-17.5 (aliquot number = 24). The dark line corresponds to the D_E value calculated using the Minimum Age Model. Both samples clearly show a significant scatter in the D_E values which may be considered as typical for fluvial sediments.

Here, D_E value of each aliquot is displayed along with its associated relative standard error and precision.

The descriptive statistics which facilitated the age model decision procedures based on [Bailey and Arnold \(2006\)](#) and the range of OSL derived D_E values are shown in [Table 5](#). [Table 5](#) also compares the D_E values derived using the MAM with the mean and the weighted

mean values. Data indicate that differences between the mean D_E value and the MAM D_E value range from 20% to almost 80%, while the weighted mean dose estimates differ from about 5% to 60% comparing to MAM D_E values. In all samples, MAM produced smaller D_E values than the mean and weighted mean values, and produced a reduction in the associated D_E errors.

Table 6 Equivalent doses, dose rates and resulting OSL-dating ages for quartz samples from the Sperchios delta plain.

Sample	D_E (Gy)	Dose rate (Gy/ka)	OSL-dating age (ka)
GT1-3	5.74 ± 0.83	2.56 ± 0.03	2.2 ± 0.3
GT1-9	12.5 ± 1.43	2.67 ± 0.04	4.7 ± 0.5
GT1-12	14 ± 1.65	2.42 ± 0.04	5.8 ± 0.7
GT1-14.5	16.9 ± 1.8	2.48 ± 0.03	6.8 ± 0.7
GT1-19.8	23 ± 2.3	2.66 ± 0.03	8.7 ± 1.1
GT2-5.7	5.4 ± 0.76	1.39 ± 0.02	3.9 ± 0.5
GT2-10.5	6.4 ± 0.22	1.09 ± 0.01	5.9 ± 0.2
GT2-14.3	11.2 ± 0.4	1.58 ± 0.02	7.1 ± 0.3
GT2-15.5	20 ± 1.1	2.29 ± 0.03	8.7 ± 0.5
GT2-17.5	35.3 ± 2.2	2.51 ± 0.04	14.1 ± 0.9
GT3-5.8	11.1 ± 1.7	2.91 ± 0.25	3.8 ± 0.6
GT3-8.1	12.6 ± 1.6	2.83 ± 0.04	4.5 ± 0.6
GT3-13.7	12.9 ± 1.8	1.88 ± 0.03	6.9 ± 1.0
GM5-1.3	1.7 ± 0.4	2.36 ± 0.03	0.7 ± 0.2
GM5-2.6	3.8 ± 0.8	2.01 ± 0.03	1.9 ± 0.4
GM5-3.8	5.3 ± 0.9	1.7 ± 0.03	3.1 ± 0.5
KR7-1	0.98 ± 0.2	1.51 ± 0.02	0.6 ± 0.1
KR7-2	1.8 ± 0.5	1.58 ± 0.02	1.1 ± 0.3
KR7-3	3.8 ± 0.7	1.43 ± 0.02	2.7 ± 0.5

4.2. Age estimates and sedimentation rates

Equivalent doses, dose rates and resulting OSL ages for all samples are given in Table 6; ages are given with 1-sigma (1σ) confidence interval, including all random and systematic uncertainties. Ages range from 14.1 ± 0.9 ka to 0.6 ± 0.1 ka and indicate an Early–Late Holocene deposition. Dating results for the five cores are in correct chronostratigraphic order (within uncertainties) as the deepest sample in each core shows the oldest age estimate. The reliability of the OSL ages can additionally be supported by independent previous chronological studies conducted in the area. ^{14}C dating on marine shells collected through coring in the region of the delta (Pechlivanidou *et al.*, 2014) gave similar ages at the corresponding depths. Particularly, core samples GT1-9 and GT3-5.8 gave ages of 4.7 ± 0.5 ka and 3.8 ± 0.6 ka respectively at depths of 3 m.b.s.l. and 3.8 m.b.s.l. They were collected at proximal (comparable) spots and similar depths to the sp1 and sp4 core samples of Pechlivanidou *et al.* (2014) at depths of 2 m.b.s.l. and 2.3 m.b.s.l. which were dated as 1403 ± 113 cal yr BP and 1778 ± 108 cal yr BP respectively, indicating a common Late Holocene deposition.

The sedimentary facies of the Sperchios delta represent transgressive to regressive sequences, overlying on Late Pleistocene–Late Holocene deposits. Terrestrial sediments probably represent fluvial sediments accumulated during the Early (8.7 ± 1.1 ka as sample GT1-19.8 shows) to Middle (6.8 ± 0.7 ka as sample GT1-14.5 shows) stages of the Holocene

regression in the south–central part of the present delta, when the rate of sea-level rise was surpassed by the sedimentation rate. In the north–central part of the basin (core GT3), terrestrial sediments (most probably fluvial) were dated as 6.9 ± 1.0 ka (sample GT3-13.7) to 3.8 ± 0.6 ka (sample GT3-5.8) representing the Middle–Late Holocene deposition. These terrestrial deposits are found from ~ 14 m.b.s.l. to ~ 8.5 m.b.s.l. in the south–central part and ~ 11.7 m.b.s.l. to ~ 3.8 m.b.s.l. in the north–central part of the Sperchios basin. Pechlivanidou *et al.* (2014) also dated fluvial sediments derived from a 40-m.b.s.l. borehole and suggested that these deposits represented the beginning of the last transgression around the Pleistocene/Holocene boundary. Further, Tziavos (1977) found that fluvial sediments developed under the present delta plain near Anthili (central part of the delta) at ~ 37 m.b.s.l., which indicate the occurrence of the Sperchios alluvial plain prior to the Holocene transgression.

Under the sea-level rising conditions and when the rate of sea-level rise outpaced sediment supply rate, the gradual flooding of the study area started. This is indicated by the presence of molluscan shell fragments, most probably suggesting a coastal/lagoon environment. The OSL ages assign these conditions from 5.8 ± 0.7 ka (sample GT1-12) to 4.7 ± 0.5 ka (sample GT1-9) for the south–central part of Sperchios basin and soon after 3.8 ± 0.6 ka (sample GT3-5.8) for the north–central part of the basin. Regarding the south part of Sperchios basin (core GT2), the total absence of molluscan shell fragments indicated that the sea did not reach this part of the basin during the last 14.1 ± 0.9 ka.

Deceleration in sea-level rise favored the progradation of the delta, as the rate of sediment supply outpaced the rate of sea-level rise. The shift back to terrestrial conditions is estimated to have started soon after 4.7 ± 0.5 ka (sample GT1-9) for the south–central part of the basin. These conditions are represented by deltaic deposits dominated by fine-grained (clay) sediments and the complete absence of molluscan shells.

For the eastern part of the basin (next to current coastline), a shift back to coastal conditions indicated by the presence of molluscan shell fragments, started at $\sim 0.6 \pm 0.1$ ka (sample KR7-1).

The data can be used to determine sedimentation rates occurred in the Sperchios delta plain; however, several limitations in such calculations exist, including factors such as surface run off and tectonic subsidence, among others, that act as substantial moderators of the sedimentation rate of an area. Nevertheless, in the present study, they cannot be

examined and incorporated in the calculations of sedimentation rates; consequently sedimentation rates provided here should be considered with caution. OSL ages are plotted against the corresponding core depth in Fig. 9. Six ages from two cores (GM5 and KR7) collected at the downstream part of the delta, in close proximity to the current coastline, define a nearly linear sedimentation rate ranging from ~0.7 mm/yr over the deepest 3 m to ~2 mm/yr over the upper 1 m.

The mean sedimentation rate for the upstream part (cores GT1, GT2 and GT3) of the basin during the Middle–Late Holocene (~7–2.2 ka) was calculated at ~2.6 mm/yr. For the south–central part of the basin (core GT1), sedimentation remains constant until ~8.7 ka (full length of the core GT1).

Despite the fact that sedimentation in the Sperchios basin is mainly controlled by sea-level variations, one might expect that the significant local tectonisms

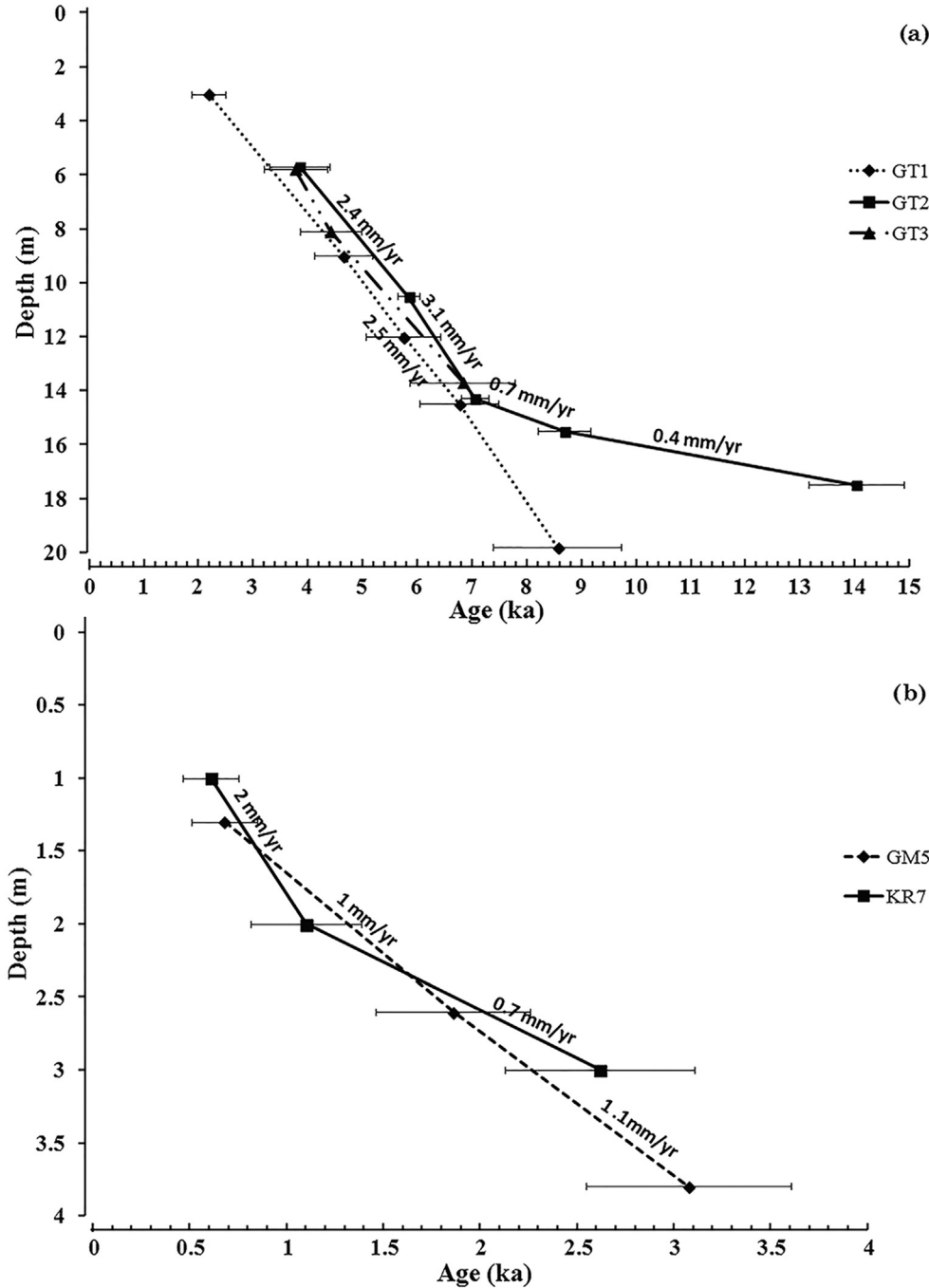


Fig. 9 Model plots of the OSL-dating age versus its corresponding core depth for (a) three cores of GT1, GT2, and GT3 at the upstream part in the Sperchios basin; and (b) two cores of GM5 and KR7 at the downstream part in the Sperchios basin. Error bars indicate one sigma uncertainty interval. A fit of the points indicates the sedimentation rate at different depths.

may have resulted in a different depositional regime and stratigraphic architecture at its southern margin. A distinct break and a large reduction by a factor of ~0.7 mm/yr sedimentation rate at ~15 m for the southern margin (core GT2) of the Sperchios basin are evident at ~7 ka (Fig. 9). Different sedimentation rates identified in core GT2 may be interpreted as the result of sediment supply from laterally sourced depositional systems which were controlled by several active normal fault segments of the Sperchios basin.

Furthermore, the striking change observed in sedimentation rates at ~7 ka may indicate the transition to terrestrial conditions and the development of the Sperchios delta plain following the deceleration in the rate of the sea-level rise recorded across the broader region of the Aegean (e.g., Stanley and Warne, 1994). This is in agreement with previous studies in this area (e.g., Pechlivanidou *et al.*, 2014) and also with studies conducted in other deltas in the Mediterranean (e.g., in the Rhone delta, Boyer *et al.*, 2005; and, in the Aliakmon delta, Styllas, 2014).

5. Conclusions

1) Since the increase of experience on effective absolute dating studies of fluvial–deltaic formations by employing the OSL technique is still on demand, the present study was mainly focused on the methodological approach that would allow accurate and precise absolute dating ages to be produced. From the depositional environment, incomplete bleaching of the samples was expected; and the methodological approach was proven from the D_E distributions and statistical parameters.

From a methodological perspective, this study suggests that: (1) the luminescence SAR approach utilizing quartz grains on small (2 mm) aliquots is a viable method to determine the burial age of deltaic deposits. And, (2) D_E distribution analysis based on statistical parameters allowed the choice of the appropriate statistical model which led to precise D_E values and to reduction of the associated age errors.

2) Furthermore, this study suggests that luminescence dating offers excellent potential for establishing a chronological framework for the depositional sequences of the Sperchios delta plain. For the first time, absolute dating information based on luminescence dating of deltaic deposits was obtained in the region.

3) The chronology for the five cores in this study shows that deltaic sediments were deposited during the Holocene. A relatively rapid deposition is implied

for the top ~14 m possibly as a result of the deceleration in the rate of the sea-level rise and the transition to terrestrial conditions, while on the deeper parts the reduced sedimentation rate may indicate a lagoonal or coastal environment.

Acknowledgements

This study has been supported by the Greek General Secretariat of Research and Technology through ESPA-KRIPIS Project: “Development of an integrated management framework of river basins and associated coastal and marine zone”.

References

- Aitken, M.J., 1985. *Thermoluminescence Dating*. Academic Press, London, p. 359.
- Amorosi, A., Centineo, M.C., Colalongo, M.L., Fiorini, F., 2005. Millennial-scale depositional cycles from the Holocene of the Po Plain, Italy. *Marine Geology*, 18, 222–223.
- Arnold, L.J., Bailey, R.M., Tucker, G.E., 2007. Statistical treatment of fluvial dose distributions from southern Colorado arroyo deposits. *Quaternary Geochronology*, 2, 162–167.
- Arnold, L.J., Roberts, R.F., Galbraith, S.B., DeLong, S.B., 2009. A revised burial dose estimation procedure for optical dating of young and modern-age sediments. *Quaternary Geochronology*, 4(4), 306–325.
- Athanassas, C., 2011. Constraints on the precision of SAR in equivalent dose estimations close to saturation in quartz. *Geochronometria*, 38(4), 413–423.
- Bailey, R.M., Arnold, L.J., 2006. Statistical modelling of single grain quartz D_E distributions and an assessment of procedures for estimating burial dose. *Quaternary Science Reviews*, 25, 2475–2502.
- Boyer, J., Duvail, C., Le Strat, P., Gensous, B., Tesson, M., 2005. High resolution stratigraphy and evolution of the Rhone delta plain during postglacial time, from subsurface drilling data bank. *Marine Geology*, 222–223, 267–298.
- Bruno, L., Amorosi, A., Severi, P., Bartolomei, P., 2015. High-frequency depositional cycles within the Late Quaternary alluvial succession of Reno River (northern Italy). *Italian Journal of Geosciences*, 134, 339–354.
- Ditlefsen, C., 1992. Bleaching of K-feldspars in turbid water suspensions: a comparison of photo- and thermoluminescence signals. *Quaternary Science Reviews*, 11, 33–38.
- Duller, G.A.T., 2008. Single-grain optical dating of Quaternary sediments: why aliquot size matters in luminescence dating. *Boreas*, 37(4), 589–612.
- Eliet, P.P., Gawthorpe, R.L., 1995. Drainage development and sediment supply within rifts, examples from the

- Sperchios basin, central Greece. *Journal of the Geological Society*, 152, 883–893.
- Fiebig, M., Preusser, F., 2007. Investigating the amount of zeroing in modern sediments of River Danube, Austria. *Quaternary Geochronology*, 2, 143–149.
- Folk, R.L., 1974. *Petrology of Sedimentary Rocks*. Hemphill Publication Company, Texas, p. 170.
- Fuchs, M., Wagner, G.A., 2003. Recognition of insufficient bleaching by small aliquots of quartz for reconstructing soil erosion in Greece. *Quaternary Science Reviews*, 22, 1161–1167.
- Galbraith, R.F., Laslett, G.M., 1993. Statistical models for mixed fission track ages. *Nuclear Tracks and Radiation Measurements*, 21(4), 459–470.
- Galbraith, R.F., Roberts, R.G., 2012. Statistical aspects of equivalent dose and error calculation and display in OSL dating: an overview and some recommendations. *Quaternary Geochronology*, 11, 1–27.
- Galbraith, R.F., Roberts, R.G., Laslett, G.M., Yoshida, H., Olley, J.M., 1999. Optical dating of single and multiple grains of quartz from Jinmium rock shelter, Northern Australia: part I, experimental design and statistical models. *Archaeometry*, 41, 339–364.
- Gartzos, E., Stamatis, G., 1996. Genesis of the thermal springs of the Sperchiosgraben, Greece. *Neues Jahrbuch für Mineralogie, Geologie und Palaontologie*, 2, 91–115.
- Guérin, G., Mercier, N., 2012. Preliminary insight into dose deposition processes in sedimentary media on a scale of single grains: Monte Carlo modelling of the effect of water on the gamma dose rate. *Radiation Measurements*, 47, 541–547.
- Guérin, G., Mercier, N., Adamiec, G., 2011. Dose-rate conversion factors: update. *Ancient TL*, 29, 5–8.
- Jacobs, Z., Roberts, R.G., 2007. Advances in optically stimulated luminescence (OSL) dating of individual grains of quartz from archaeological deposits. *Evolutionary Anthropology*, 16, 210–223.
- Kilias, A.A., Tranos, M.D., Papadimitriou, E.E., Karakostas, V.G., 2008. The recent crustal deformation of the Hellenic orogen in central Greece; the Kremasta and Sperchios Fault Systems and their relationship with the adjacent large structural features. *Zeitschrift der Deutschen Gesellschaft für Geowissenschaften*, 159(3), 533–547.
- Kraft, J., Rapp, G., Szemler, G., Tziavos, Ch, Kase, E., 1987. The pass of Thermopylae, Greece. *Journal of Field Archaeology*, 14, 181–198.
- Kunz, A., Pflanz, D., Weniger, T., Urban, B., Krüger, F., Chen, Y.G., 2013. Optically stimulated luminescence dating of young fluvial deposits of the Middle Elbe River Flood Plains using different age models. *Geochronometria*, 41, 36–56.
- Lafuerza, S., Canals, M., Casamor, J.L., Devincenzi, J.M., 2005. Characterization of deltaic sediment bodies based on *in situ* CPT/CPTU profiles: a case study on the Llobregat delta plain, Barcelona, Spain. *Marine Geology*, 222–223, 497–510.
- Lambeck, K., Purcell, A., 2005. Sea-level change in the Mediterranean Sea since the LGM: model predictions for tectonically stable areas. *Quaternary Science Reviews*, 24, 1969–1988.
- Lepper, K., McKeever, S.W.S., 2002. An objective methodology for dose distribution analysis. *Radiation Protection Dosimetry*, 101, 349–352.
- Madsen, A.T., Murray, A.S., Andersen, T.J., Pejrup, M., Breuning-Madsen, H., 2005. Optically stimulated luminescence dating of young estuarine sediments: a comparison with ^{210}Pb and ^{137}Cs dating. *Marine Geology*, 214, 251–268.
- Marinos, G., Anastopoulos, I., Maratos, G., Melidonis, N., Andronopoulos, B., 1963. *Geological Map of Greece 1:50000 — Sheet STYLIDA*. Institute of Geology and Mineral Exploration, Athens, Greece.
- Marinos, G., Anastopoulos, I., Maratos, G., Melidonis, N., Andronopoulos, B., Papastamatiou, I., Tataris, A., Vetoulis, D., Mpornovas, I., Katsikatsos, G., Maragoudakis, N., Lalexos, N., 1967. *Geological Map of Greece 1:50000 — Sheet LAMIA*. Institute of Geology and Mineral Exploration, Athens, Greece.
- Maroukian, H., Lagios, E., 1987. Neotectonic movements in the Sperchios River Basin, central Greece. *Zeitschrift für Geomorphologie*, 63, 133–140.
- Munsell Color Company, 1994. *Munsell Soil Color Charts — Revised Edition*. Macbeth Division of Kollmorgen, New Windsor.
- Murray, A.S., Wintle, A.G., 2000. Luminescence dating of quartz using an improved single-aliquot regenerative-dose protocol. *Radiation Measurements*, 32, 57–73.
- Murray, A.S., Wintle, A.G., 2003. The single aliquot regenerative dose protocol: potential for improvements in reliability. *Radiation Measurements*, 37, 377–381.
- Nathan, R.P., Mauz, B., 2008. On the dose-rate estimate of carbonate-rich sediments for trapped charge dating. *Radiation Measurements*, 43, 14–25.
- Olley, J., Caitcheon, G., Murray, A., 1998. The distribution of apparent dose as determined by optically stimulated luminescence in small aliquots of fluvial quartz: implications for dating young sediments. *Quaternary Science Reviews*, 17, 1033–1040.
- Olley, J., Caitcheon, G., Roberts, R.G., 1999. The origin of dose distribution in fluvial sediments, and the prospect of dating single grains from fluvial deposits using optically stimulated luminescence. *Radiation Measurements*, 30, 207–217.
- Olley, J., De Deckker, P., Roberts, R.G., Fifield, L.K., Yoshida, H., Hancock, G., 2004a. Optical dating of deep-sea sediments using single grains of quartz: a comparison with radiocarbon. *Sedimentary Geology*, 169, 175–189.
- Olley, J., Pietsch, T., Roberts, R.G., 2004b. Optical dating of Holocene sediments from a variety of geomorphic settings using single grains of quartz. *Geomorphology*, 60, 337–358.
- Pavlopoulos, K., 2010. Relative sea level fluctuations in Aegean coastal areas from middle to late Holocene. *Geodynamica Acta*, 23(5–6), 225–232.
- Pavlopoulos, K., Kapsimalis, V., Theodorakopoulou, K., Panagiotopoulos, I., 2012. Vertical displacement trends in the Aegean coastal zone (NE Mediterranean) during the Holocene assessed by geo-archaeological data. *The Holocene*, 22, 717–728.
- Pechlivanidou, S., Vouvalidis, K., Løvlie, R., Nesje, A., Albanakis, K., Pennos, C., Syrides, G., Cowie, P.,

- Gawthorpe, R., 2014. A multi-proxy approach to reconstructing sedimentary environments from the Sperchios delta, Greece. *The Holocene*, 24(12), 1825–1839.
- Pirazzoli, P.A., 1996. *Sea-Level changes: the last 20,000 YEARS (Coastal Morphology and Research)*. Wiley, New York, p. 207.
- Poulos, S., Leontaris, S., Collins, M.B., 1997. Sedimentological and clay mineralogical investigations in Maliakos Gulf, eastern Greece. *Bollettino Di Geofisica Teorica Ed Applicata*, 38(3–4), 267–279.
- Prescott, J.R., Hutton, J.T., 1988. Cosmic ray and gamma ray dosimetry for TL and ESR. *International Journal of Radiation Applications and Instrumentation. Part D Nuclear Tracks and Radiation Measurements*, 14, 223–227.
- Prescott, J.R., Hutton, J.T., 1994. Cosmic ray contributions to dose rates for luminescence and ESR dating: large depths and long-term time variations. *Radiation Measurements*, 23, 497–500.
- Prescott, J.R., Stephan, L.G., 1982. The contribution of cosmic radiation to the environmental dose for thermoluminescent dating. Latitude, altitude and depth dependences. *Council of Europe Journal PACT*, 6, 17–25.
- Preusser, F., Degering, D., Fuchs, M., Hilgers, A., Kadereit, A., Klasen, N., Krbetschek, M., Richter, D., Spencer, J.Q.G., 2008. Luminescence dating: basics, methods and applications. *Journal of Quaternary Science*, 57, 95–149.
- Rendell, H.M., Webster, S.E., Sheffer, N.L., 1994. Underwater bleaching of signals from sediment grains: new experimental data. *Quaternary Science Reviews*, 13, 433–435.
- Rittenour, T., 2008. Luminescence dating of fluvial deposits: applications to geomorphic, palaeoseismic and archaeological research. *Boreas*, 37, 613–635.
- Roberts, R.G., Galbraith, R.F., Olley, J.M., Yoshida, H., Laslett, G.M., 1999. Optical dating of single and multiple grains of quartz from Jinmium rock shelter, northern Australia: part II, results and implications. *Archaeometry*, 41, 365–395.
- Rodnight, H., Duller, G.A.T., Wintle, A.G., Tooth, S., 2006. Assessing the reproducibility and accuracy of optical dating of fluvial deposits. *Quaternary Geochronology*, 1, 109–120.
- Somoza, L., Barnolas, A., Arasa, A., Maestro, A., Rees, J.G., Hernandez-Molina, F.J., 1998. Architectural stacking patterns of the Ebro delta controlled by Holocene high frequency eustatic fluctuations, delta-lobe switching and subsidence processes. *Sedimentary Geology*, 117, 11–32.
- Stanley, D.J., Warne, A., 1994. Worldwide initiation of Holocene marine deltas by deceleration of sea level rise. *Science*, 265, 228–231.
- Stokes, S., Bray, H.E., Blum, M.D., 2001. Optical resetting in large drainage basins: tests of zeroing assumptions using single-aliquot procedures. *Quaternary Science Reviews*, 20, 879–885.
- Styllas, M., 2014. A simple approach for defining Holocene sequence stratigraphy using borehole and cone penetration test data. *Sedimentology*, 61, 444–460.
- Theodorakopoulou, K., Pavlopoulos, K., Thriantaphyllou, M., Kouli, K., Tsourou, T., Bassiakos, Y., Zacharias, N., Hayden, B., 2009. Geoarchaeological studies in the coastal area of Istron–Kalo Chorio (Gulf of Mirabello–Eastern Crete): landscape evolution and paleoenvironmental reconstruction. *Zeitschrift fur Geomorphologie*, 53, 55–70.
- Trauerstein, M., Lowick, S.E., Preusser, F., Veit, H., 2017. Testing the suitability of dim sedimentary quartz from northern Switzerland for OSL burial dose estimation. *Geochronometria*, 44, 66–76.
- Tsakalos, E., Christodoulakis, J., Charalambous, L., 2016. The Dose Rate calculator (DRc) — A Java application for dose rate and age determination based on luminescence and ESR dating. *Archaeometry*, 58, 347–352.
- Tziavos, C., 1977. *Sedimentology, Ecology and Paleogeography of the Sperchios Valley and Maliakos Gulf, Greece*. Master Thesis. University of Delaware.
- Vouvalidis, K., Syrides, G., Albanakis, K., 2005. Holocene morphology of the Thessaloniki Bay: impact of sea level rise. *Zeitschrift fur Geomorphologie*, 137, 147–158.
- Vouvalidis, K., Syrides, G., Pavlopoulos, K., Papakonstantinou, M., Tsourlos, P., 2010b. Holocene palaeoenvironmental changes in Agia Paraskevi prehistoric settlement, Lamia, central Greece. *Quaternary International*, 216, 64–74.
- Vouvalidis, K., Syrides, G., Pavlopoulos, K., Pechlivanidou, S., Tsourlos, P., Papakonstantinou, M., 2010a. Palaeogeographical reconstruction of the battle terrain in Ancient Thermopylae, Greece. *Geodinamica Acta*, 23(5–6), 241–253.
- Wallinga, J., 2002. Optically stimulated luminescence dating of fluvial deposits: a review. *Boreas*, 31, 303–322.
- Wallinga, J., Bos, I.J., 2010. Optical dating of fluvio-deltaic clastic lake-fill sediments — A feasibility study in the Holocene Rhine delta (western Netherlands). *Quaternary Geochronology*, 5, 602–610.
- Wallinga, J., Hobo, N., Cunningham, A.C., Versendaal, A.J., Makaske, B., Middelkoop, H., 2010. Sedimentation rates on embanked floodplains determined through quartz optical dating. *Quaternary Geomorphology*, 5, 170–175.
- Wintle, A.G., Murray, A.S., 2006. A review of quartz optically stimulated luminescence characteristics and their relevance in single aliquot regeneration dating protocols. *Radiation Measurements*, 41(4), 369–391.
- Zacharias, N., Bassiakos, Y., Hayden, B., Theodorakopoulou, K., Michael, C.T., 2009. Luminescence dating of deltaic deposits from Eastern Crete, Greece: geoarchaeological implications. *Geomorphology*, 109, 46–53.